Paper submitted August 1982

Eddy Current Probe Design Using Finite Element Analysis*

by N. Ida, R. Palanisamy, and W. Lord

Abstract

The use of eddy current probes is widespread in the nuclear industry, but although significant advances in modeling of electromagnetic fields and nondestructive testing (NDT) phenomena have been achieved, little attention has been given to the design and modeling of the probes themselves. This paper describes the use of the finite element method to the design of absolute and differential eddy current probes. Comparison is made with experimental data obtained with a variable size—variable spacing differential probe. Also studied is the effect of the coil size on the probe's ability to distinguish between closely spaced discontinuities.

INTRODUCTION

The use of eddy current probes is widespread in the nuclear industry for periodic testing of nuclear power plant steam generators. Both absolute and differential eddy current probes are used at a variety of operating frequencies depending on the materials encountered in each testing situation and the properties or defects of interest. Although some of these probes are commercially available, little attention has been given in the literature to the design and modeling of the probes themselves.

The successful use of the finite element method for analysis of dc and low frequency electromagnetic fields in electrical machinery[1-3] was soon followed by applications in the NDT field.[4-9] The basic properties of the finite element method (in particular the ease of handling boundary conditions), ability to follow awkward shapes, and the relative economy of com-

*This work has been supported by the Electric Power Research Institute under Project RP 1395-2.

Nathan Ida was born in Rumania on December 12, 1949. He received his B.Sc. and M.Sc. in electrical engineering from Ben-Gurion University, Beer Sheva, Israel, in 1977 and 1979, respectively, and his Ph.D. in electrical engineering from Colorado State University in 1983. He is currently a research assistant professor with the Department of Electrical Engineering at Colorado State University, Fort Collins, CO, and is working on numerical modeling of electromagnetic NDT phenomena. Ida is a member of the IEEE Magnetics Society.

R. Palanisamy received his B.Sc. in physics and his B.E. and M.Sc. in electrical engineering from the University of Madras, India, and his M.E. in mechanical engineering from Howard University. He is currently on leave from the Propulsion Engineering Division of the Indian Space Research Organization, Trivandrum, India, working for his Ph.D. in electrical engineering at Colorado State University on the numerical solution of nonlinear, time varying, electromagnetic field problems.

William Lord graduated from Nottingham University, U.K., with a B.Sc. (Hons.) and Ph.D. in electrical engineering. He has taught at the University of Tennessee, Clarkson College of Technology, and most recently at Colorado State University, where he is a professor of electrical engineering. His current NDT research interests are in the modeling of magnetic phenomena for defect characterization. For inquiries concerning this work, contact the author at (303) 491-6018.

0025-5327/83/$2.00/0

puter facilities make it a particularly attractive method for modeling of electromagnetic NDT phenomena.

This paper describes the application of a numerical model, based on an axisymmetric finite element formulation to the design of absolute and differential eddy current probes. First, a standard differential eddy current probe is analyzed by varying the size of the coils and the spacing between them. The signals calculated are compared with experimental data obtained with a specially built variable coil size/variable spacing differential probe. Next, the effect of the coil size on the probe's ability to distinguish between closely spaced discontinuities is studied for an absolute eddy current probe. These results show clearly the importance of the coil size and the coil's spacing in relation to the defect size or the spacing between discontinuities. Large coils tend to produce a composite signal, thus masking the effect of individual discontinuities, while closely spaced coils (in the case of differential probes) produce signals with reduced amplitude. Best results are obtained with coils whose size and spacing are of the same order of magnitude as the discontinuities themselves.

THE FINITE ELEMENT MODEL

The differential equation governing eddy current phenomena in regions that include conducting and magnetic materials can be written as

$$\frac{1}{\mu}(\nabla\times\nabla\times\bar{A})=\bar{J}_s-\sigma\frac{\partial\bar{A}}{\partial t}, \tag{1}$$

where μ, $\bar{A}$,$\bar{J}_s$, and σ are the magnetic permeability (H/m), magnetic vector potential (Weber/m), applied current density vector in the coil (A/m^2), and the electrical conductivity (mhos/m), respectively. In the case of a single frequency (ω rad/s), continuous wave, as is the case in many eddy current testing situations, Equation 1 reduces to

$$\left(\frac{1}{\mu}\right)\nabla^2\bar{A}=-\bar{J}_s+j\omega\sigma\bar{A}. \tag{2}$$

Solution to this linear diffusion equation for the sinusoidal steady-state condition can be obtained in terms of $\bar{A}$ by solving Equation 2 with appropriate boundary conditions. From the values of $\bar{A}$, one can obtain any observable electromagnetic phenomena such as coil impedance changes, energy dissipation, flux densities, etc.

Many practical eddy current NDT geometries are axisymmetric as the excitation coils are circular. An absolute or differential probe over a conducting plane, a feed-through probe in a conducting tube, and an encircling probe system around a conducting rod are some of the geometries satisfactorily analyzed in a simplified cylindrical coordinate system (r,θ,z). In this system, both $\bar{J}_s$ and $\bar{A}$ have components only in the positive θ direction. That is, they are functions of r and z only. Hence, in the case of axisymmetric geometries, Equation 2 reduces to

$$\frac{1}{\mu}\left(\frac{\partial^2\bar{A}}{\partial r^2}+\frac{1}{r}\frac{\partial\bar{A}}{\partial r}+\frac{\partial^2\bar{A}}{\partial z^2}-\frac{\bar{A}^2}{r^2}\right)=-\bar{J}_s+j\omega\sigma\bar{A}. \tag{3}$$

The finite element method does not offer a solution to the diffusion equation directly.[10] Instead, the solution is obtained at discrete points (nodes) in the solution region by formulating an energy functional equivalent to Equation 3 and minimizing it with respect to an approximate function space, thus solving the resulting simultaneous algebraic equations for the unknown magnetic vector potential values at each point in the region. The assumptions made in this process are:

(1) The source current density, $\bar{J}_s$, and the magnetic vector potential, $\bar{A}$, vary sinusoidally with time. In other words, both can be described as phasors. Harmonics are absent both in the impressed and induced currents and fields.

(2) Eddy currents within the excitation coils can be neglected. That is, the ac resistance of an eddy current coil is constant and equal to its dc resistance.

(3) Electrical conductivity and magnetic permeability are single-valued in each element in the solution region. Thus, field dependency of the permeability is neglected although spatial variations in μ are possible.

(4) The displacement currents as well as any volume or surface charge densities are neglected.

These assumptions are quite mild and fully justified at the excitation levels and frequencies encountered in NDT applications; therefore, the resulting numerical model is a powerful and valuable tool in NDT.

ENERGY FUNCTIONAL AND FINITE ELEMENT FORMULATION

As pointed out earlier, an energy functional equivalent to the diffusion equation (Equation 3) is formulated based on the energy balance in the solution region.

$$F=\int_v(\text{stored energy}+\text{dissipated energy}-\text{input energy})dv. \tag{4}$$

Or, in terms of the magnetic field, the magnetic vector potential, and applied current density, this can be written as[2,3]

$$F(A)=\int_v\left[\frac{1}{\mu}BdB+\frac{1}{2}j\omega\sigma\left|A\right|^2-J_s\cdot A\right]dv. \tag{5}$$

In axisymmetric situations, the magnetic vector potential has a single component along the θ axis as is the case for the current density. Furthermore, because these are constant in the θ direction, a unit depth is assumed in the formulation. The functional can now be written in terms of $\bar{A}$ as a surface integral:

$$F(\bar{A})=\int_R\int\left[\frac{1}{2\mu}\left\{\left|\frac{\partial\bar{A}}{\partial z}\right|^2+\left|\frac{\partial\bar{A}}{\partial r}+\frac{\bar{A}}{r}\right|^2\right\}+\frac{j\omega\sigma}{2}\left|\bar{A}\right|^2-\bar{J}_s\cdot\bar{A}\right]r\,dr\,dz, \tag{6}$$

where the first term represents the stored energy in the magnetic field, the second represents the dissipated energy through eddy currents, and the third is the input energy. The solution now consists of finding a set of functions $\bar{A}$ such that the energy-related functional is minimized.

Because this cannot be done everywhere in space, a bounded region (solution region) is discretized into a large number of linear triangular elements. In each element, three nodal points are defined at which the magnetic vector potential is found. The value of $\bar{A}$ within each element is assumed to be a linear combination of the nodal values A_i.[3]

$$A(r,z)=\frac{1}{2\Delta}\sum_{i=1}^{3}(a_i+b_ir+c_iz)A_i, \tag{7}$$

where Δ is the area of the element, and A_i are the nodal values of the magnetic vector potential. This approximation is extended throughout the solution region resulting in N nodal points and therefore in N unknown values of A.

Minimization of the energy functional is achieved by setting the partial derivative with respect to each nodal value equal to zero:

$$\frac{\partial F(A)}{\partial A_k}=0 \qquad k=1,2,\ldots,N. \tag{8}$$

The approximation for the magnetic vector potential in Equation 7 is substituted into the energy functional and the derivatives with respect to the three nodes set to zero. This results in three equations that in matrix form can be written as

$$[[S]_e+j[R]_e]\{A\}_e=\{Q\}_e. \tag{9}$$

$[S]$ is the 3×3 real part of the elemental matrix consisting of geometrical quantities of the mesh (r and z values of the ele-

ment vertices, the area of the element, and permeability) and represents the left hand side of Equation 3. $[R]$ is the 3×3 imaginary part of the matrix and consists of the values of conductivity (σ), angular frequency (ω), and area of the element and represents the second term in the right hand side of Equation 3. $\{Q\}$ is the 3×1 vector of contributions at the nodes of the element from the impressed current densities (J_s), and $\{A\}$ is the 3×1 vector of unknown values of the magnetic vector potential at the nodes of the element.

This elemental system of equations is the basic finite element representation of the energy functional. Each such elemental matrix is summed into a global system of equations

$$[G]\{A\}=\{Q\}, \tag{10}$$

where $[G]$ is the $N\times N$ banded symmetric complex global matrix, and $\{Q\}$ and $\{A\}$ are the $N\times 1$ complex source matrix and the $N\times 1$ complex vector of unknowns, respectively.

The Gauss elimination algorithm is applied to this system of equations, taking advantage of the symmetry and bandwidth, to solve for A at the nodes of the finite element mesh.

From the magnetic vector potential, other quantities can be calculated such as flux densities and coil impedances.

IMPEDANCE OF EDDY CURRENT COILS

In NDT applications, the signals from eddy current probes carry information concerning the environment of the probes, changes in which cause variations in the probe impedance. The coil impedance can be calculated directly from the complex magnetic vector potential.[8] The impedance of a circular loop of radius r_i carrying a current I_s is

$$\bar{z}_i=\frac{j\omega 2\pi r_i \bar{A}_i}{\bar{I}_s}, \tag{11}$$

where A_i is the value of the magnetic vector potential at r_i.

Integration of this equation over the cross section of the coil yields the impedance of the coil. Because the values of A are not known at the location of each turn in the coil, an average value is taken as representing the magnetic vector potential in each element. This value is associated with the centroid of the element, the radius of the loop being r_c. Then, assuming N_s to be a uniform turn density, the impedance of the coil is

$$Z_{\text{coil}}=-\frac{j\omega 2\pi N_s}{I_s}\sum_{j=1}^{N} r_{cj}A_{cj}\Delta_j, \tag{12}$$

or, because $N_sI_s=J_s$,

$$Z_{\text{coil}}=-\frac{j\omega 2\pi J_s}{I_s^2}\sum_{j=1}^{N}(r_{cj}\Delta_j)A_{cj}, \tag{13}$$

where N is the number of elements in the cross section of the coil.

In situations where differential eddy current probes are used, two identical coils carrying the same current are present. The impedance of the probe is found calculating the impedance of each coil using Equation 13 and summing them to find the total impedance:

$$Z_{\text{probe}}=\frac{j\omega 2\pi J_s}{I_s^2}\left[\sum_{j=1}^{N_b}(r_{cj}\Delta_j)A_{cj}-\sum_{j=1}^{N_a}(r_{cj}\Delta_j)A_{cj}\right], \tag{14}$$

where Na and Nb are the number of elements in coils a and b, respectively.

RESULTS

The finite element method described above was applied to the analysis of a differential eddy current probe as shown in Fig. 1a. In this situation, both the spacing and the width of the coils can be varied. The depth of the coils, denoted by c in Fig. 1a, is such as to allow a constant current density in the coils as the coil width increases (i.e., the cross-sectional area of each coil remains constant).

The geometry in Fig. 1a is discretized into a number of triangular elements, as shown in Fig. 1b. The finite element method is now applied to solve for the magnetic vector potential at each of the nodes of the mesh in Fig. 1b. From these values, the impedance of the coil is calculated at discrete points (probe position) to form a plot called an "impedance plane trajectory."

In this case, advantage is taken of the fact that symmetry exists about the z axis and therefore only half of the geometry is analyzed. Also, because symmetry also exists about the center of the defect, the probe is allowed to move up to the point where it is centered with the defect, and the impedance values calculated are reflected to form a full impedance plane trajectory.

Figure 2 compares the experimental (Fig. 2a) and finite element results (Fig. 2b) from a differential probe with coils 0.08 in. (2.032 mm) wide at spacings between 0.04 to 0.34 in. (1.016 to 8.636 mm). The defect shown in Fig. 1a is 0.04 in. (1.016 mm) wide and 0.015 in. (0.381 mm) deep, on the outer surface of a ⅞ in. (22.225 mm) Inconel 600 tube.

The experimental results were obtained using a special probe, as shown in Fig. 3. Figure 3a shows the probe body and spacers used to vary the spacing. Figure 3b shows the three different coil sizes used, and Fig. 3c shows an assembled probe with one of the coil sets. Figure 3d is the experimental arrangement used, showing a probe, Inconel tube, and the drive unit used to move the probe.

These results show clearly that, as the spacing of the coils increases, the resulting impedance plane trajectory loses its differential nature, and the probe behaves increasingly as two distinct absolute probes. On the other hand, decreasing the spacing widens the loops but also reduces the amplitude of the trajectories.

Figure 4 compares different sized coils at a constant spacing for the same defect described in the previous paragraph. The

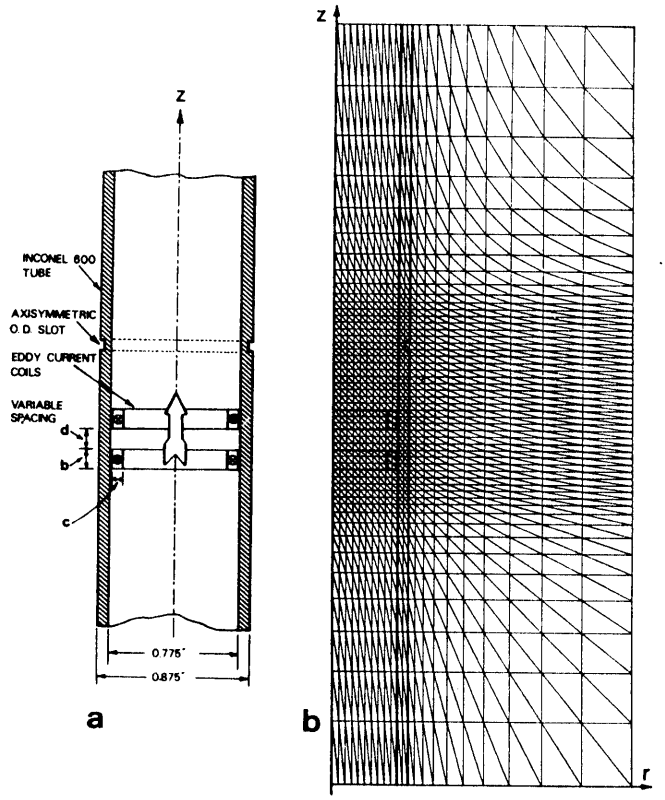

Figure 1—Differential eddy current probe inside a tube with an OD axisymmetric slot: (a) geometry and (b) finite element mesh (half region).

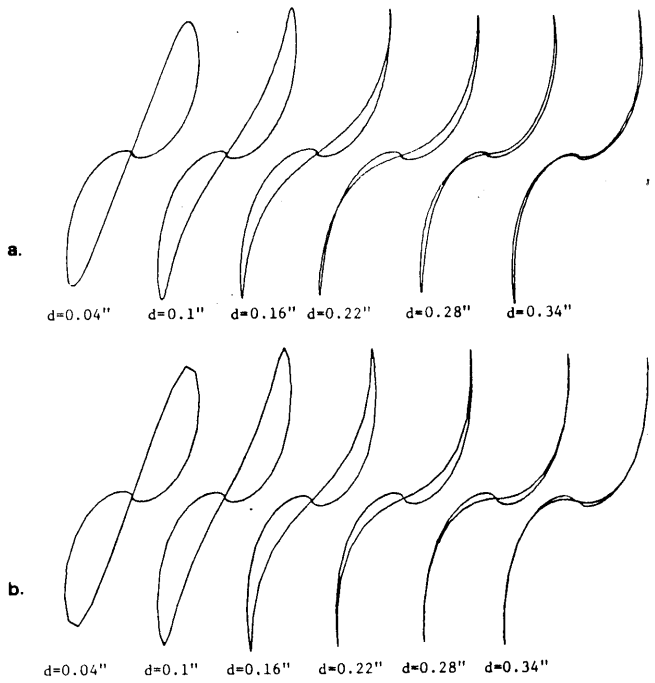

Figure 2—Comparison of impedance plane trajectories for different coil spacing at 100 kHz (coil width is 0.080 in. [2.032 mm]): (a) experimentally recorded and (b) finite element predictions (for OD axisymmetric slot 0.04 in. [1.016 mm] wide and 0.015 in. [0.381 mm] deep in an Inconel tube).

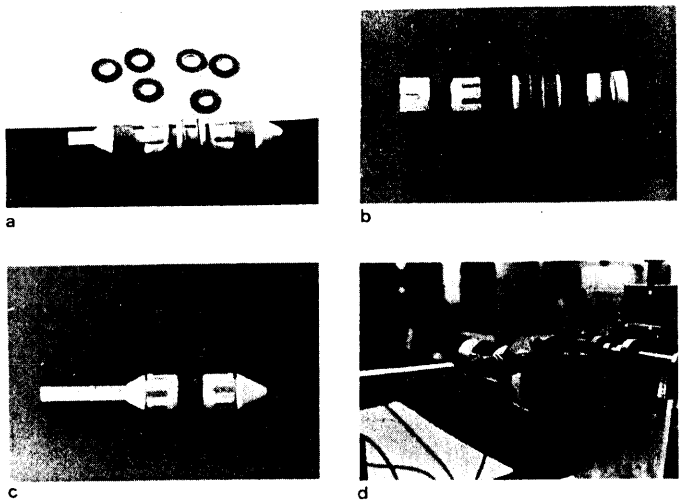

Figure 3—Photograph of (a) probe body and spacers, (b) coils, (c) assembled probe, and (d) tube, probe, and the drive unit.

spacing is 0.1 in. (2.54 mm), and the coil width varies from 0.02 to 0.3 in. (0.508 to 7.62 mm). In this case, as the coil becomes wider, the amplitude increases and the shape becomes narrower. From these calculations and experiments, it is clear that a good compromise is achieved by choosing a probe whose coil width and spacing is comparable to the width of the defect.

Further finite element predictions were made to illustrate the potential use of this model as a design tool. Impedance plane trajectories were calculated and plotted by varying the following parameters in a given probe.

(1) Frequency: The impedance plane trajectories were calculated at 50, 100, and 150 kHz.

(2) Defect geometry: Two different defects were simulated; one, a 0.04 in. (1.016 mm) wide and 0.015 in. (0.381 mm) deep outside diameter (OD) defect, and the second a 0.04 in. (1.016 mm) wide and 0.030 in. (0.762 mm) deep OD defect.

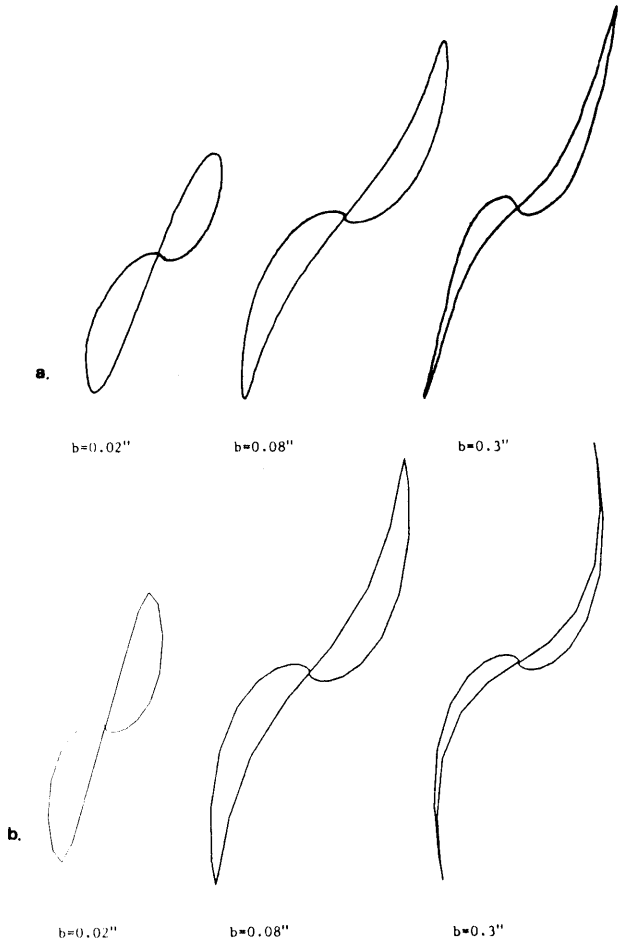

Figure 4—Comparison of impedance plane trajectories for different coil sizes at 100 kHz (constant spacing of 0.10 in. [2.54 mm]): (a) experimentally recorded and (b) finite element predictions for the same slot as in Fig. 2.

(3) Coil spacing; the calculations above were performed at coil spacings of 0.04, 0.10, 0.16, 0.22, 0.28 and 0.34 in. (1.016, 2.54, 4.064, 5.588, 1.991, and 8.636 mm). These calculations are plotted in Fig. 5. These plots also show the relation in the amplitude for smaller and larger defects and the importance of choosing the correct spacing for the probe coil if meaningful signals are to be obtained.

As a second example of the application of the finite element method to probe modeling, the geometry in Fig. 6 was studied. It is a section of a steam generator's Incoloy 800 tube inside the tube sheet region. The steam generator (German design) has rolled tubes where the rolling region can be at varying distances from the tube sheet inner surface (l in Fig. 6). The absolute coil, 1 mm thick, has a length of l mm, which needs to be optimized for the particular application. In addition, the signal from the rolling region is to be modeled for identification of the tube condition.

To determine the probe length needed to obtain the best signal for different locations of the rolling region relative to the tube sheet surface, three coil lengths (a=1, 3, and 9 mm) were modeled each for three distances (l=1, 3, and 9 mm). The finite element results for these nine situations are plotted in Fig. 7.

It is clear from this figure that the longer the coil in comparison with the distance between the two factors that cause the change in the signal (tube sheet and rolling region), the less distinct are the two phenomena in the signal. Thus, a coil, 9 mm long, testing for the rolling region, which is only 1 mm away from the tube sheet surface, produces a flat composite signal in which the rolling and the tube sheet cannot be dis-

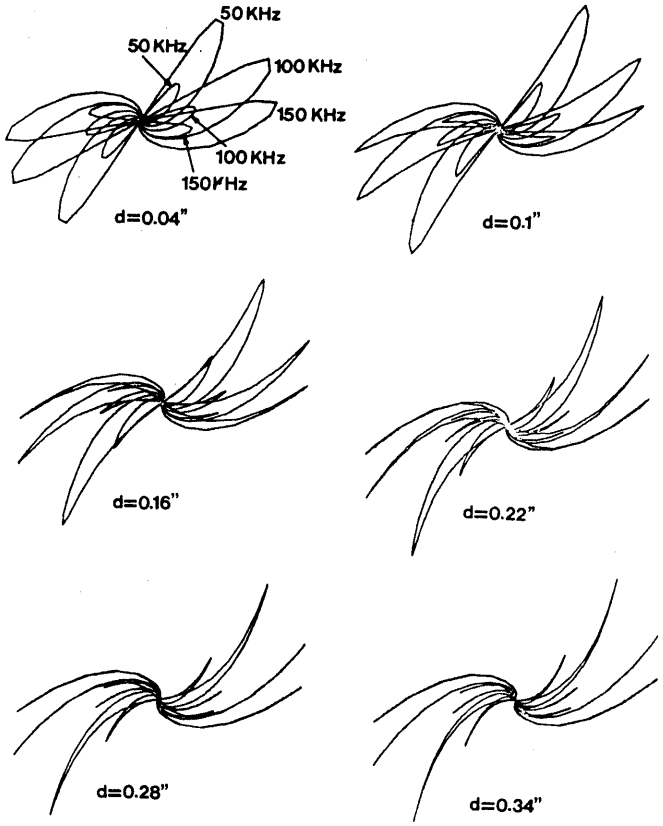

Figure 5—Finite element predicted impedance plane trajectories for different defects, frequencies, and coil spacings. (Small signals are for an OD axisymmetric slot 0.04 in. [1.016 mm] wide and 0.015 in. [0.381 mm] deep. The larger signals are for a similar slot 0.04 in. [1.016 mm] wide and 0.03 in. [0.762 mm] deep.)

tinguished, as in Fig. 7g. The other extreme is when the coil is much smaller than the distance, as in Fig. 7c. Here the two signals are simply superimposed, as one signal does not affect the other.

The curves in Fig. 4 are generated at 100 kHz and are, in general, a composite signal. The lower, comma-shaped part of the curve is due to the effect of the tube sheet and the upper, "s" shaped part is due to the rolling region. These curves compare very well with experimental results, such as the curve in Fig. 8, taken at 100 kHz. The choice of coil shape might be complicated by additional factors, such as the minimum number of required turns, but as can be seen from these results, the coil should be of the same general length as the effect it is measuring. Because the average distance of the rolling region is about 3 mm, a coil length of 3 mm would be a good choice.

CONCLUSIONS

The finite element method, originally developed for studying electromagnetic fields in electrical machinery, can be used with significant advantages to observe eddy current NDT phenomena. In particular, the numerical modeling of probes for the purpose of probe optimization in testing situations is of significant importance for the nuclear industry where heavy reliance on eddy current probes is encountered. In some instances, the numerical process is the only feasible way to analyze the testing situation, such as in the case of subsurface defects. This paper describes the application of the numerical model under simple axisymmetric conditions. For the more general, arbitrarily shaped defect geometries in steam generators or other nonaxisymmetric situations, a more complex three-dimensional model is required. It is, however, clear from this work

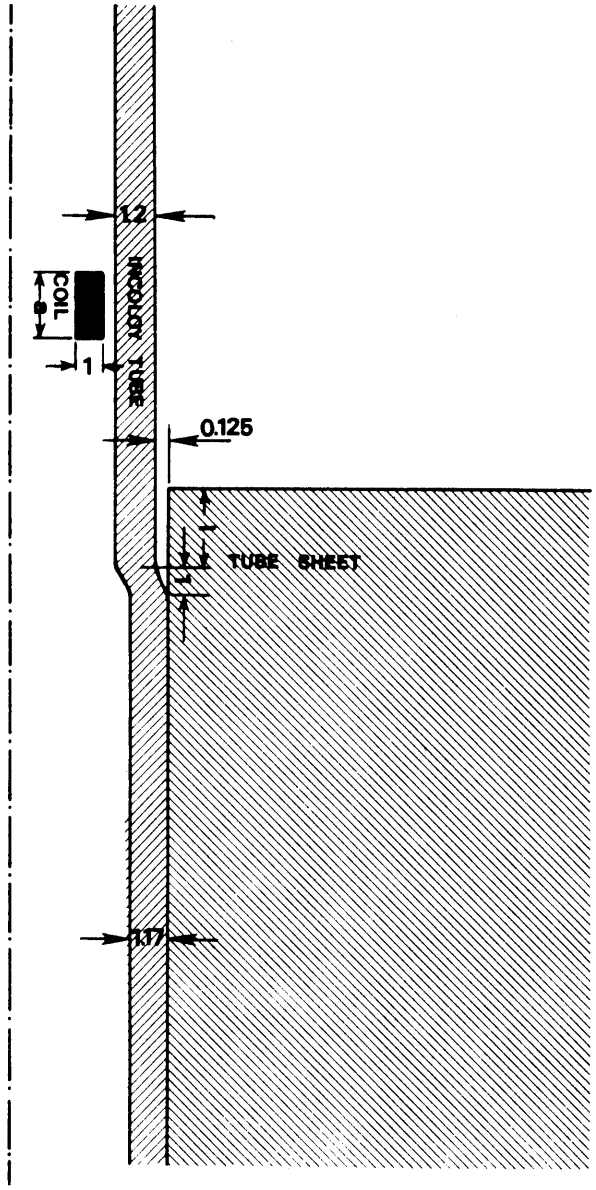

Figure 6—Geometry of steam generator section showing the tube sheet, tube, and coil. Dimensions are in millimeters.

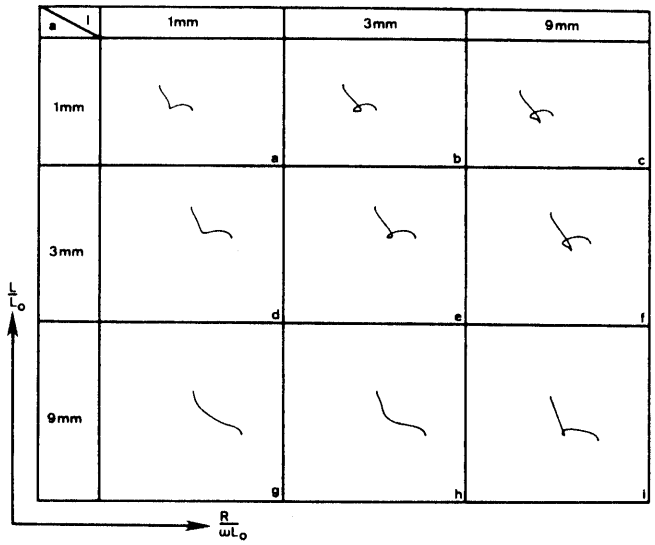

Figure 7—Impedance plane trajectories of different coils (1, 3, and 9 mm long) and different spacings between tube sheet and rolling (1, 3, and 9 mm).

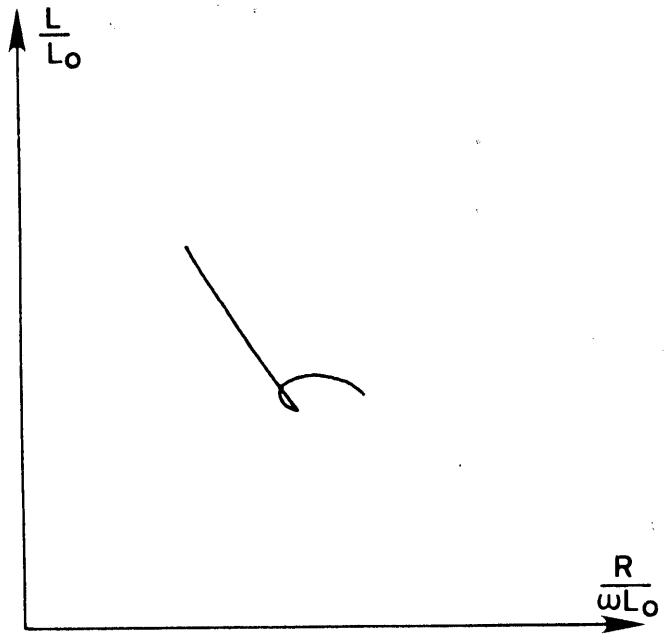

Figure 8—Experimental impedance plane trajectory from a 3 mm long coil at nominal spacing of the tube sheet and rolling at 100 kHz.

that significant improvements can be made in the design of eddy current probes with regard to testing situations using available numerical models.

References

1. Donea, J., S. Giulinai, and A. Philippe, "Finite Elements in the Solution of Electromagnetic Induction Problems," *International Journal for Numerical Methods in Engineering*, Vol. 8, 1974, pp 359–367.
2. Silvester, P., and M. V. K. Chari, "Finite Element Solution of Saturable Magnetic Field Problems," *IEEE Transactions on Power Apparatus and Systems*, Vol. 89, 1970, pp 1642–1651.
3. Anderson, O. W., "Transformer Leakage Flux Program Based on the Finite Element Method," *IEEE Transactions on Power Apparatus and Systems*, Vol. 92, March–April 1973, pp 682–689.
4. Lord, W., and J. H. Hwang, "Finite Element Modeling of Magnetic Field Defect Interactions," *ASTM Journal of Testing and Evaluation*, Vol. 3, No. 1, Jan. 1975, pp 21–25.
5. Lord, W., and J. H. Hwang, "Defect Characterization from Magnetic Leakage Fields," *British Journal of Nondestructive Testing*, Vol. 19, No. 1, Jan. 1977, pp 14–18.
6. Lord, W., J. M. Bridges, W. Yen, and R. Palanisamy, "Residual and Active Leakage Fields Around Defects in Ferromagnetic Materials," *Materials Evaluation*, Vol. 36, No. 8, July 1978, pp 47–54.
7. Lord, W., "A Survey of Electromagnetic Methods of Nondestructive Testing," *Mechanics of Nondestructive Testing*, edited by W. W. Stinchcomb, 1980, pp 77–100. Plenum Press, New York, NY.
8. Palanisamy, R., and W. Lord, "Finite Element Modeling of Electromagnetic NDT Phenomena," *IEEE Transactions on Magnetics*, Vol. MAG–15, No. 6, Nov. 1979, pp 1479–1481.
9. Ida, N., K. Betzold, and W. Lord, "Finite Element Modeling of Absolute Eddy Current Probe Signals," accepted for publication in the *Journal of Nondestructive Evaluation*.
10. Chari, M. V. K., "Finite-element Solution of the Eddy-current Problem in Magnetic Structures," *IEEE Transactions on Power Apparatus and Systems*, Vol. PAS–93, No. 1, Jan.–Feb. 1974, pp 62–72.